Discrete repulsive oscillator wavefunctions

2009 J. Phys. A: Math. Theor. 42 485210

(http://iopscience.iop.org/1751-8121/42/48/485210)

IOP PUBLISHING JOURNAL OF PHYSICS A: MATHEMATICAL AND THEORETICAL

J. Phys. A: Math. Theor. **42** (2009) 485210 (12pp) doi:10.1088/1751-8113/42/48/485210

Discrete repulsive oscillator wavefunctions

Carlos A Muñoz, Juvenal Rueda-Paz and Kurt Bernardo Wolf

Instituto de Ciencias Físicas, Universidad Nacional Autónoma de México, Av. Universidad s/n, Cuernavaca, Morelos 62251, Mexico

E-mail: bwolf@fis.unam.mx

Received 28 August 2009
Published 17 November 2009
Online at stacks.iop.org/JPhysA/42/485210

Abstract

For the study of infinite discrete systems on phase space, the three-dimensional Lorentz algebra and group, so(2,1) and SO(2,1), provide a discrete model of the repulsive oscillator. Its eigenfunctions are found in the principal irreducible representation series, where the compact generator—that we identify with the position operator—has the infinite discrete spectrum of the integers $\mathcal{Z}$, while the spectrum of energies is a double continuum. The right- and left-moving wavefunctions are given by hypergeometric functions that form a Dirac basis for $\ell^2(\mathcal{Z})$. Under contraction, the discrete system limits to the well-known quantum repulsive oscillator. Numerical computations of finite approximations raise further questions on the use of Dirac bases for infinite discrete systems.

PACS numbers: 02.20.Qs, 02.30.Mv, 02.60.Cb, 02.70.Bf, 03.65.Sq

1. Introduction

Our interest presently lies in building discrete Hamiltonian models, i.e. those where position is a discrete variable, with equally spaced values, finite or infinite in number. The discrete models should have the same geometry and dynamics, determined by their two Hamilton equations, as the continuous models of quadratic Hamiltonian systems: the harmonic oscillator, the free particle and the repulsive—or *inverted*—oscillator characterized by a potential barrier $-\frac{1}{2}x^2$. By embedding the discrete and continuous models in the same Lie algebra, properties of the latter are expected to have precise counterparts in the former.

The discrete harmonic oscillator [1, 2] is ruled by the unitary Lie algebra su(2) = so(3) and answers questions on its discrete wavefunctions, such as finite signals and pixellated images [3, 4]; their phase space (for one-dimensional signals) is a sphere. Next, *infinite* discrete signals in a free system are ruled by the Euclidean algebra iso(2) [5], and their phase space is a cylinder. In this paper, a discrete model of the repulsive oscillator is built with the three-dimensional Lorentz algebra so(2,1) = su(1,1), within a representation of the principal series; phase space should be a one-sheeted hyperboloid (to be explored in the next paper).

The signals are functions of integer positions and can have a continuum of energies, both above and under the potential barrier $-\frac{1}{2}x^2$. The treatment of infinite signals presents further issues on representation, approximation and asymptotics that will be pointed as we proceed.

We regard a one-dimensional discrete Hamiltonian system as composed by the following elements: a designated compact *position* operator $\mathcal{X}$, whose spectrum $\{x_m\}$ is discrete, and a *Hamiltonian* operator $\mathcal{H}$. The Lie bracket of these two operators defines the *momentum* operator through $\mathcal{P} := -\mathrm{i}[\mathcal{H}, \mathcal{X}]$. We further propose that these three operators close into a Lie algebra; here $\{\mathcal{X}, \mathcal{P}, \mathcal{H}\}$ will close into the Lorentz algebra $\mathsf{so}(2,1)$. We shall show that this provides a family of discrete analogues of the one-dimensional classical and quantum repulsive oscillator.

From the theory of unitary irreducible representations of the algebra $\mathsf{so}(2,1)$ [6], we know that the spectrum of the compact (timelike) generator is equally spaced and, according to the Hilbert space chosen, are infinite $m \in \mathcal{Z} := \{0, \pm 1, \pm 2, \ldots\}$ in the *principal* representation series, and semi-infinite $m \in \mathcal{Z}_k^{\pm} := \pm\{k, k{+}1, k{+}2, \ldots\}$ in the *complementary* series. (We use the nomenclature of Naĭmark and Gel'fand [7, 8] because in Bargmann's designation [6] they are called the 'continuous' and 'discrete' representation series, names that could be confusing in our context.)

The quantum repulsive oscillator is rather well known; it was studied by G Barton in his PhD thesis, published in [9], where travel and tunneling delay times are analyzed with coherent states, and all important previous references are given. Balazs and Voros [10] analyzed the phase space aspects of tunneling using the Wigner function. The construction of the quantum wavefunctions can be found in [12] and [11, sections 7.5.11–15] among others, while modern applications are considered in [13–17]. The properties of the classical and quantum models are gathered in section 2. In section 3, we introduce the discrete model on the Lorentz Lie algebra and recall the standard construction of its unitary irreducible representations. The eigenfunctions of the discrete model are found in section 4 as overlaps between the position and energy bases, and given by the solutions to a three-term difference equation that has analytic solutions. In section 5, we offer some strategies to handle these infinite discrete function bases in the necessarily finite numerical computations. In the concluding section 6, we discuss some lines for future research.

2. Classical and quantum continuous models

Classical models regard the observables of position, momentum, energy and unit, $\{x, p, h, 1\}$ under Poisson brackets $\{\cdot, \cdot\}$, while quantum models regard the corresponding self-adjoint operators $\{\widehat{X}, \widehat{P}, \widehat{H}, \widehat{1}\}$ under Lie brackets (here commutators $[\cdot, \cdot]$) in the Hilbert space $\mathcal{L}^2(\mathsf{R})$. In these terms, the geometric and dynamic Hamilton equations of the repulsive oscillator are

$$\begin{array}{lll} & \text{Classical} & \text{Quantum} \\ \text{Hamiltonian:} & h := \frac{1}{2}(p^2 - x^2), & \widehat{H} := \frac{1}{2}(-\mathrm{d}^2/\mathrm{d}x^2 - x^2), \\ \text{geometric:} & \{h, x\} = -p, & [\widehat{H}, \widehat{X}] = -\mathrm{i}\widehat{P}, \\ \text{dynamic:} & \{h, p\} = -x, & [\widehat{H}, \widehat{P}] = -\mathrm{i}\widehat{X}, \\ \text{basic:} & \{x, p\} = 1 \text{ center}, & [\widehat{X}, \widehat{P}] = \mathrm{i}\widehat{1} \text{ center}. \end{array} \tag{1}$$

The three brackets define the Lie algebra $\mathsf{wso}(1,1)$ containing $\mathsf{so}(1,1)$ boosts of phase space, with a Heisenberg–Weyl ideal w. This is the Lie algebra that we intend to deform (or 'precontract') to $\mathsf{so}(2,1)$.

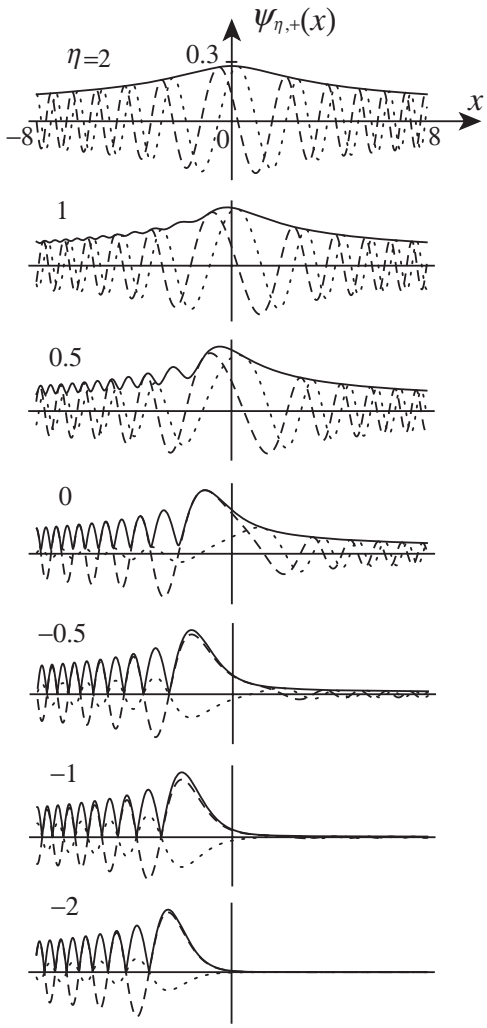

Figure 1. Quantum mechanical eigenfunctions of the (continuous) repulsive oscillator $\psi_{\eta,+}(x)$ in (3), for $x \in [-8, 8]$ and $\eta \in \{2, 1, 0.5, 0, -0.5, -1, -2\}$. Dashed, dotted and continuous lines show the real, imaginary and absolute values of the function.

The spectrum and eigenfunctions of the Hamiltonian of the quantum repulsive oscillator are known to be [12]

$$\widehat{H}\,\psi_{\eta,\pm}(x) = \eta\,\psi_{\eta,\pm}(x), \qquad \psi_{\eta,+}(x) = \psi_{\eta,-}(-x), \qquad \eta, x \in \mathsf{R}, \tag{2}$$

$$\psi_{\eta,\pm}(x) = \frac{\exp[\mathrm{i}14\pi(12 - \mathrm{i}\eta)]}{2^{3/4}\pi}\Gamma\left(\frac{1}{2} - \mathrm{i}\eta\right) D_{-\frac{1}{2}+\mathrm{i}\eta}(\pm \mathrm{e}^{\mathrm{i}3\pi/4}\sqrt{2}\,x), \tag{3}$$

where $D_{-\frac{1}{2}+\mathrm{i}\eta}(z) = U(-\mathrm{i}\eta, z)$ is the parabolic cylinder function [18, vol 2, p 119], [19, chapter19]. These functions are plotted in figure 1 for various values of the energy η (see [11, figure 7.11]), where we can see that solutions (3) multiplied by the phase $\exp(-\mathrm{i}\eta t)$ represent the time evolution of right-moving waves over the potential barrier ($\eta > 0$), because the real

and imaginary parts of the function are off by approximately $\frac{1}{4}$-cycle; the absolute values are time invariant. Below the barrier ($\eta < 0$) and to its left ($x < 0$), the absolute values develop a series of maxima and come very close to zero; this indicates 'almost-standing' waves produced from the interference between the incoming waves and those reflected off the potential barrier; the part that tunnels through continues to be a small right-moving wave. Finally, we note that they have a chirping asymptotic behavior, $\psi_{\eta,\pm}(x) \sim \mathrm{e}^{\mathrm{i}x^2/2}/\sqrt{|x|}$ for $|x| \to \infty$ [19, equation 19.8.1], and are Dirac-orthonormal.

3. Discrete systems based on so(2,1)

We postulate that the three classical observables, x, p, λ, of position, momentum and a displaced or proportional energy $\lambda \propto \eta +$ constant (that we will call *pseudo*-energy), are the spectra of the generators of an so(2,1) algebra. This algebra is defined by the abstract commutation relations between its three generators, $\mathcal{L}_0$, $\mathcal{L}_1$ and $\mathcal{L}_2$, as follows:

$$[\mathcal{L}_0, \mathcal{L}_1] = -\mathrm{i}\mathcal{L}_2, \qquad [\mathcal{L}_1, \mathcal{L}_2] = +\mathrm{i}\mathcal{L}_0, \qquad [\mathcal{L}_2, \mathcal{L}_0] = -\mathrm{i}\mathcal{L}_1. \tag{4}$$

The + sign in the second commutator stresses that the $\mathcal{L}_0$-axis has a different metric from that of $\mathcal{L}_1$- and $\mathcal{L}_2$-axes.

We propose the following correspondences between the classical observables and the so(2,1) generators:

$$\text{position } x \leftrightarrow \mathcal{X} = \mathcal{L}_0, \tag{5}$$

$$\text{momentum } p \leftrightarrow \mathcal{P} = \mathcal{L}_1, \tag{6}$$

$$\text{pseudo-energy } \lambda \leftrightarrow \mathcal{L} = \mathcal{L}_2. \tag{7}$$

Then, from (4), they will satisfy the commutation relations

$$[\mathcal{L}, \mathcal{X}] = -\mathrm{i}\mathcal{P}, \qquad [\mathcal{L}, \mathcal{P}] = -\mathrm{i}\mathcal{X}, \qquad [\mathcal{X}, \mathcal{P}] = -\mathrm{i}\mathcal{L}, \tag{8}$$

where we recognize that the first two brackets are the geometric and dynamic Hamilton equations in (1), while the third is the 'nonstandard' basic commutator that determines the deformation to our discrete model.

We proceed now to repeat succinctly the construction and classification of the abstract so(2,1) algebra irreducible representations [6, 20] with the raising and lowering operators

$$\mathcal{L}_\uparrow := \mathcal{L}_2 + \mathrm{i}\mathcal{L}_1, \qquad \mathcal{L}_\downarrow := \mathcal{L}_2 - \mathrm{i}\mathcal{L}_1. \tag{9}$$

(Other authors such as [21] use a $\frac{1}{2}\pi$-rotated version of these, $\mathcal{L}_1 \pm \mathrm{i}\mathcal{L}_2$; at the end, however, (9) will lead to simpler wavefunctions with a single hypergeometric function.) Their commutators are

$$[\mathcal{L}_0, \mathcal{L}_{\uparrow\downarrow}] = \pm\mathcal{L}_{\uparrow\downarrow}, \qquad [\mathcal{L}_\uparrow, \mathcal{L}_\downarrow] = -2\mathcal{L}_0, \tag{10}$$

the invariant Casimir operator is

$$\mathcal{C} := \mathcal{L}_1^2 + \mathcal{L}_2^2 - \mathcal{L}_0^2 = \mathcal{L}_{\uparrow\downarrow}\mathcal{L}_{\downarrow\uparrow} - \mathcal{L}_0(\mathcal{L}_0 \mp I), \tag{11}$$

and the eigenvalues γ of $\mathcal{C}$ will determine the distinct self-adjoint representations of so(2,1). But while in su(2) the value of the Casimir operator suffices to determine uniquely the representation and eigenvalue ranges of all generators [22], in so(2,1) there can be more than one irreducible representation in certain ranges of γ.

The states of the discrete repulsive oscillator model are the discrete wavefunctions, or *signals* $f_m \equiv f(x_m)$, $m \in \mathcal{Z}$, which live in the Hilbert space $\ell^2(\mathcal{Z})$ of square-summable sequences with the usual inner product $(f, g) := \sum_{m\in\mathcal{Z}} f_m^* g_m = (g, f)^*$ and

norm $|f| = \sqrt{(f, f)}$. In this space, the generators (5)–(7) and the Casimir operator (11) should be self-adjoint—and their spectra real—while the raising and lowering operators in (9) are the adjoints of each other. There is a natural Kronecker basis for $\ell^2(\mathcal{Z})$ given by the simultaneous eigenvectors of position $x_m = m$ and of the Casimir operator,

$$\mathcal{L}_0 f_m^\gamma = m f_m^\gamma, \qquad m \in \mathcal{Z}, \qquad \mathcal{C} f_m^\gamma = \gamma f_m^\gamma, \qquad \gamma \in \mathsf{R}, \tag{12}$$

that correspond to infinite column vectors of 0's with a single 1 in position m. From so(2,1) theory [6], we know that for the compact generator $\mathcal{L}_0$ to have *integer* eigenvalues, the exponentiated Lie group must be SO(2,1); its two-fold cover SU(1, 1) has also half-integer values, and its universal cover $\overline{\mathsf{SO}}(2, 1)$ can have any equally spaced spectra.

Because of the first of (10), the raising and lowering operators (9) acting on f_m^γ will yield another eigenvector of $\mathcal{L}_0$ corresponding to the eigenvalue one unit above and below,

$$\mathcal{L}_{\uparrow\downarrow} f_m^\gamma = c_{\uparrow\downarrow m}^\gamma f_{m\pm1}^\gamma, \tag{13}$$

up to normalization constants $c_{\uparrow\downarrow m}^\gamma$ that must be found, but whose phase is arbitrary. The constraints on the ranges of γ and m are found through a well-known line of reasoning [6]:

$$0 \leqslant \left|c_{\uparrow\downarrow m}^\gamma\right|^2 \left(f_{m\pm1}^\gamma, f_{m\pm1}^\gamma\right) = \left(\mathcal{L}_{\uparrow\downarrow} f_m^\gamma, \mathcal{L}_{\uparrow\downarrow} f_m^\gamma\right) = \left(f_m^\gamma, \mathcal{L}_{\downarrow\uparrow}\mathcal{L}_{\uparrow\downarrow} f_m^\gamma\right) \tag{14}$$

$$= \left(f_m^\gamma, \left[\mathcal{C} + \mathcal{L}_0^2 \pm \mathcal{L}_0\right] f_m^\gamma\right)$$

$$= (\gamma + m^2 \pm m)\left(f_m^\gamma, f_m^\gamma\right), \tag{15}$$

$$\Longrightarrow \left|c_{\uparrow\downarrow m}^\gamma\right|^2 = \gamma + m^2 \pm m \geqslant 0. \tag{16}$$

Hence, if some $c_{\downarrow m_{\min}}^\gamma = 0$, the equally spaced spectrum of $\mathcal{X} = \mathcal{L}_0$ will be bounded from below by $m_{\min}$ (positive complementary series); if $c_{\uparrow m_{\max}}^\gamma = 0$, it is bounded from above by $m_{\max}$ (negative complementary series). The former were used in [23] to discretize the square-radius coordinate of a polar array of 'sensor-points' on a plane with constant angular number. Here, however, the case of our interest requires that $c_{\uparrow\downarrow m}^\gamma$ never be zero, so that the position spectrum will be $m \in \mathcal{Z}$.

It is convenient to now introduce the *Bargmann* representation index k [6], related to the Casimir eigenvalue γ by

$$\gamma = k(1-k), \qquad \left(k - \frac{1}{2}\right)^2 = 14 - \gamma, \qquad k = \frac{1}{2} \pm \sqrt{14 - \gamma}, \tag{17}$$

$$\text{equation (16)} \Rightarrow |c_{\uparrow\downarrow m}^\gamma|^2 = \left(m \pm \frac{1}{2}\right)^2 - \left(k - \frac{1}{2}\right)^2 \geqslant 0. \tag{18}$$

The replacement (17) entails a square root that allows us to extract the two series of so(2,1) representations of our present interest determined by $\gamma \in \mathsf{R}$: the principal and the (positive) complementary representation series (in Bargmann's nomenclature, the continuous C_γ^0 and discrete D_k^+ series). The structure of so(2,1) representations is richer than what is presented here—we exclude negative complementary and exceptional representation series—and forego the general theory, which is adequately covered in [6, 24]. We divide the solutions of (18) into these two series:

$$\text{Principal: } \gamma \geqslant 14, \qquad k = \tfrac{1}{2} + \mathrm{i}\kappa, \qquad \kappa \in \mathsf{R}, \qquad m \in \mathcal{Z}, \tag{19}$$

$$\text{Complementary: } \gamma < 14, \qquad k \in \{1, 2, \ldots\}, \qquad m \in \mathcal{Z}_k^+. \tag{20}$$

Within each, the spectra of the three operators (5)–(7) are [24, 25]

$$\begin{array}{lll} & \text{Principal } C^0_{\gamma(k)} & \text{Complementary } D^+_k \\ \text{Spectrum of } \mathcal{C}\text{:} & \gamma = 14{+}\kappa^2, \quad \kappa \in \mathsf{R}, & \gamma = k(1{-}k),\ k \in \mathcal{Z}^+ \\ \text{Spectrum of } \mathcal{X}\text{:} & x_m = m \in \mathcal{Z}, & x_m = m \in \mathcal{Z}_0^+ + k \\ \text{Spectra of } \mathcal{L} \text{ (and } \mathcal{P})\text{:} & \lambda \in \mathsf{R} \oplus \mathsf{R}, & \lambda \in \mathsf{R} \\ \text{Spectra of } \mathcal{X}{\pm}\mathcal{P}\text{:} & \xi \in \mathsf{R}, & \xi \in \mathsf{R}^+. \end{array} \tag{21}$$

We restrict ourselves henceforth to the principal series $k = \frac{1}{2} + \mathrm{i}\kappa$ of SO(2,1) in (19), where $m \in \mathcal{Z}$. In this case, the action of the raising and lowering operators on the Kronecker eigenbasis of position is written as

$$\mathcal{L}_{\uparrow\downarrow} f^k_m = \sqrt{\left(m \pm \frac{1}{2}\right)^2 + \kappa^2}\, f^k_{m\pm 1}. \tag{22}$$

To conclude this section, we contract our discrete repulsive oscillator model to the classical and quantum models (1). In the principal series representation determined by $\kappa \in \mathsf{R}$, we rescale and shift the so(2,1) operators through

$$\mathcal{X}_\kappa := \mathcal{X}/\sqrt{\kappa}, \qquad \mathcal{P}_\kappa := \mathcal{P}/\sqrt{\kappa}, \qquad \mathcal{L}_\kappa := \mathcal{L} + \kappa 1. \tag{23}$$

When $\kappa \to \infty$, the geometric and dynamic Hamilton equations in (8) between $\mathcal{X}_\kappa, \mathcal{P}_\kappa, \mathcal{L}_\kappa$ remain invariant, while the third becomes the Heisenberg commutator, weakly in the space of wavefunctions of finite energy,

$$[\mathcal{X}_\kappa, \mathcal{P}_\kappa] = \frac{1}{\kappa}[\mathcal{X}, \mathcal{P}] = -\frac{\mathrm{i}}{\kappa}(\mathcal{L}_\kappa - \kappa 1) \underset{\kappa\to\infty}{\longrightarrow} \mathrm{i}1. \tag{24}$$

To recover the form of the quantum repulsive oscillator Hamiltonian in (1), we write the Casimir operator (11), $\mathcal{C} = \gamma 1$, with $\gamma = \frac{1}{4} + \kappa^2$ to find its limit when $\kappa \to \infty$,

$$\begin{aligned} (14 + \kappa^2)1 &= \mathcal{P}^2 + \mathcal{L}^2 - \mathcal{X}^2 = \kappa \mathcal{P}_\kappa^2 + (\mathcal{L}_\kappa - \kappa 1)^2 - \kappa \mathcal{X}_\kappa^2 \\ &= \kappa\left(\mathcal{P}_\kappa^2 - 2\mathcal{L}_\kappa - \mathcal{X}_\kappa^2\right) + \mathcal{L}_\kappa^2 + \kappa^2 1, \end{aligned} \tag{25}$$

$$\Longrightarrow \mathcal{P}_\kappa^2 - 2\mathcal{L}_\kappa - \mathcal{X}_\kappa^2 = \left(14 1 - \mathcal{L}_\kappa^2\right)/\kappa \underset{\kappa\to\infty}{\longrightarrow} 0, \tag{26}$$

$$\Longrightarrow \lim_{\kappa\to\infty} \mathcal{L}_\kappa - \frac{1}{2}\left(\mathcal{P}_\kappa^2 - \mathcal{X}_\kappa^2\right) = 0. \tag{27}$$

We thus identify the pseudo-energy generator $\mathcal{L}_\kappa$ for $\kappa \to \infty$ with the repulsive oscillator Schrödinger Hamiltonian through

$$\widehat{H} = \frac{1}{2}(\widehat{P}^2 - \widehat{X}^2) \leftrightarrow \lim_{\kappa\to\infty} \mathcal{L}_\kappa = \mathcal{L} + \lim_{\kappa\to\infty} \kappa. \tag{28}$$

On the left we have the quantum operator whose spectrum is the energy $\eta \in \mathsf{R}$, which we thus relate to the previous 'pseudo-energy' eigenvalues λ of $\mathcal{L}$ by

$$\eta = \lambda + \kappa \qquad \text{(energy)}, \tag{29}$$

and we assume this identification for all values of $\kappa \in \mathsf{R}$.

4. Difference equation and analytic solutions

In (12) we defined the Kronecker eigenbasis of position, and now we introduce the eigenbasis of energy. The simultaneous eigenstates of the pseudo-energy operator $\mathcal{L}$ and of the Casimir

operator (12) in the principal series representation labeled by κ (for $k = \frac{1}{2}+\mathrm{i}\kappa$ and $\gamma = \frac{1}{4}+\kappa^2$) are

$$\mathcal{L}h^{\kappa}_{\lambda,\sigma} = \lambda h^{\kappa}_{\lambda,\sigma}, \qquad \lambda \in \mathsf{R}, \qquad \mathcal{C}h^{\kappa}_{\lambda,\sigma} = (14+\kappa^2)h^{\kappa}_{\lambda,\sigma}, \qquad \kappa \in \mathsf{R}, \tag{30}$$

with σ an extra dichotomic index that will distinguish between the two R's in (21).

The overlap between the eigenbases of position $\{f^{\kappa}_m\}_{m\in\mathcal{Z}}$ in (12), and of energy $\{h^{\kappa}_{\lambda,\sigma}\}_{\lambda\in\mathsf{R}}$, recalling (29), defines the wavefunctions of the discrete repulsive oscillator as

$$\Psi^{\kappa}_{\lambda,\sigma}(m) = \left(f^{\kappa}_m,\, h^{\kappa}_{\lambda,\sigma}\right). \tag{31}$$

These wavefunctions satisfy a recurrence relation obtained from (9) and (22):

$$\lambda\Psi^{\kappa}_{\lambda,\sigma}(m) = \left(f^{\kappa}_m, \mathcal{L}h^{\kappa}_{\lambda,\sigma}\right) = \frac{1}{2}\left([\mathcal{L}_{\uparrow}+\mathcal{L}_{\downarrow}]f^{\kappa}_m, h^{\kappa}_{\lambda,\sigma}\right) \tag{32}$$

$$= \frac{1}{2}\sqrt{\left(m+\frac{1}{2}\right)^2+\kappa^2}\,\Psi^{\kappa}_{\lambda,\sigma}(m+1) \tag{33}$$

$$+\frac{1}{2}\sqrt{\left(m-\frac{1}{2}\right)^2+\kappa^2}\,\Psi^{\kappa}_{\lambda,\sigma}(m-1), \tag{34}$$

and this leads to the three-term real difference equation in position $m \in \mathcal{Z}$,

$$\sqrt{\left(m+\frac{1}{2}\right)^2+\kappa^2}\,\Psi^{\kappa}_{\lambda,\sigma}(m+1) - 2\lambda\Psi^{\kappa}_{\lambda,\sigma}(m) + \sqrt{\left(m-\frac{1}{2}\right)^2+\kappa^2}\,\Psi^{\kappa}_{\lambda,\sigma}(m-1) = 0. \tag{35}$$

As for second-order differential equations, the difference equation (35) has two independent solutions, to be labeled by σ. These solutions can be produced by giving two sets of 'initial' values, say at $\Psi^{\kappa}_{\lambda}(0)$ and $\Psi^{\kappa}_{\lambda}(1)$ with different ratios. Solutions corresponding to distinct eigenvalues λ will be Dirac-orthogonal, as can be seen using the argument familiar from the adjunction of operators in $\ell^2(\mathcal{Z})$ on the difference equation (35), which implies that $(\lambda-\lambda')(\Psi_{\lambda}, \Psi_{\lambda'}) = 0$. However, the resolution of the two solutions by σ is left open. One criterion, definite parity under reflections across the center $m = 0$, can be used to produce two orthogonal solutions: odd ones from $\Psi^{\kappa}_{\lambda,-}(1) = -\Psi^{\kappa}_{\lambda,-}(-1)$ and $\Psi^{\kappa}_{\lambda,-}(0) = 0$, and even ones from $\Psi^{\kappa}_{\lambda,+}(1) = \Psi^{\kappa}_{\lambda,+}(-1) = \lambda\Psi^{\kappa}_{\lambda,+}(0)/\sqrt{\gamma}$, so that $(\Psi_{\lambda,+}, \Psi_{\lambda,-}) = 0$. However, parity has not been the choice in the continuous case (3) in figure 1.

Using previous results on the $\mathsf{SO}(2,1)$ mixed-basis representations [24, equation (4.14)], we can identify analytic special functions that satisfy the difference equations (4)–(35), through the change of functions:

$$\Psi^{\kappa}_{\lambda,\sigma}(m) = \mathrm{i}^{\sigma m}\frac{\left|\Gamma\left(\frac{1}{2}+\mathrm{i}\kappa+\sigma m\right)\right|}{\Gamma(1-\mathrm{i}\lambda+\sigma m)}\Phi^{\kappa}_{\lambda,\sigma}(m), \qquad \sigma = \pm 1. \tag{36}$$

We can then verify that $\Phi^{\kappa}_{\lambda,\sigma}(m)$ satisfies one of the three-term Gaussian relations of the hypergeometric function ${}_2F_1\left[\begin{smallmatrix} a, & b \\ & c \end{smallmatrix}; z\right]$ in the parameter c for $z = \frac{1}{2}$ [26, equation 9.137.1]. We can thus declare the discrete repulsive oscillator wavefunctions to be

$$\Psi^{\kappa}_{\lambda,\sigma}(m) = c^{\kappa}_{\lambda}\,\mathrm{i}^{\sigma m}\frac{\left|\Gamma\left(\frac{1}{2}+\mathrm{i}\kappa+\sigma m\right)\right|}{\Gamma(1-\mathrm{i}\lambda+\sigma m)}\;{}_2F_1\left[\begin{matrix}\frac{1}{2}-\mathrm{i}\kappa-\mathrm{i}\lambda, & \frac{1}{2}+\mathrm{i}\kappa-\mathrm{i}\lambda \\ & 1-\mathrm{i}\lambda+\sigma m\end{matrix}; \frac{1}{2}\right], \tag{37}$$

where c^{κ}_{λ} are normalization constants that are independent of the space coordinate m, to be determined up to a phase. We note the following relations between the wavefunctions:

$$\Psi^{\kappa}_{\lambda,+}(m) = \Psi^{-\kappa}_{\lambda,+}(m) = \Psi^{\kappa}_{\lambda,-}(-m). \tag{38}$$

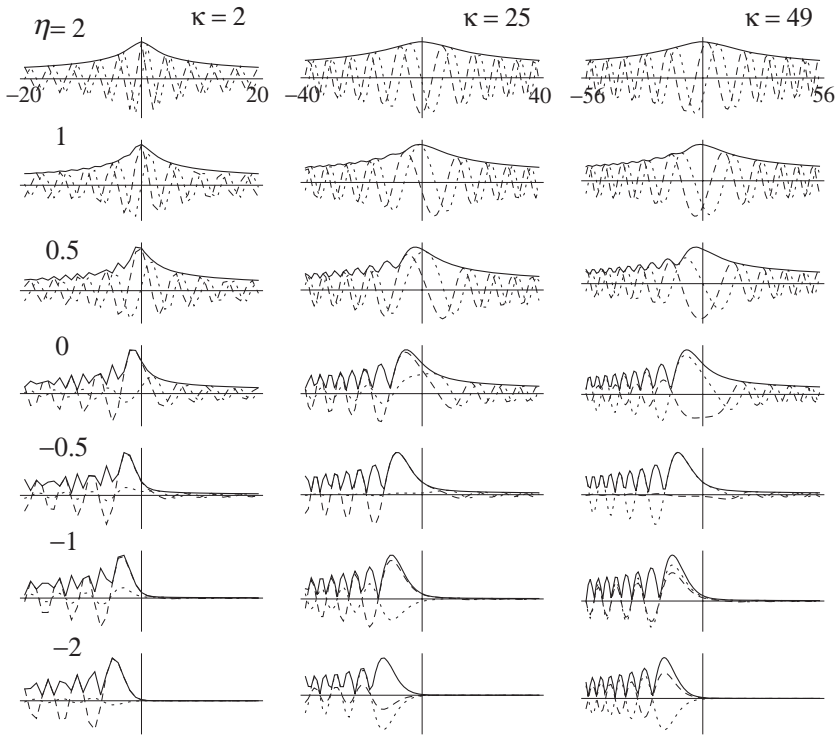

Figure 2. Discrete repulsive oscillator wavefunctions, $\Psi^{\kappa}_{\lambda,+}(m)$ in (37). Columns: representations $\kappa = 2$, 25 and 49. Rows: energies $\eta = \lambda + \kappa = 2$, 1, 0.5, 0, -0.5, -1 and -2, as in the previous figure. Dashed, dotted and continuous lines join the real, imaginary and absolute values of the function between integer points. In the last two columns, the ranges of positions $m \in \mathcal{Z}$ are $[-8, 8]$ scaled by the factor $\sqrt{\kappa}$ (i.e. 5 and 7 respectively) so that as κ grows, the discrete wavefunctions contract to the continuous repulsive oscillator ones in $[-8, 8]$ shown in the previous figure.

In figure 2 we show the discrete repulsive oscillator wavefunctions for various energies $\eta = \lambda + \kappa$. And again we can resort to the argument we made for figure 1 that they represent right-moving waves.

Although we cannot identify the discrete repulsive oscillator wavefunctions (37) with any named special function, we should point out that when in the three-term difference equation (35) the Bargmann index k is restored, the radicands become $(m \pm k)(m \mp k \pm 1)$; when $k > \frac{1}{2}$, the solutions will belong to the complementary series, with lower- and upper-bound discrete positions m. A model where this is the spectrum of a radial variable was elaborated in [23] and written in terms of Meixner polynomials $M_n(\xi; 2k, \gamma)$, where $n \in \mathcal{Z}_0^+$ counts the energy levels and is the degree of the polynomial in the discrete radial coordinate $\xi \in \mathcal{Z}_0^+$, and $\gamma \in [0, 1)$ is a contraction parameter. The hypergeometric function (37) at $z = \frac{1}{2}$, written in terms of two hypergeometrics at $1/(1 - z) = 2$, yields expressions which can be compared with the result in [23]: the degree n of the Meixner polynomial is here $\mathrm{i}\lambda - \frac{1}{2} \pm \mathrm{i}\kappa$, the discrete radial position ξ appears now as $-\sigma m - \frac{1}{2} \pm \mathrm{i}\kappa$—not polynomials, but analytic extensions of them, $2k = 1 \pm 2\mathrm{i}\kappa$ as expected—and $\gamma = -1$. Alternatively, writing the hypergeometric in the argument $z^{-1} = 2$, we find two hypergeometrics that can be identified as Kravchuk functions $K_n(x; \frac{1}{2}; 2j)$ of the finite harmonic oscillator model of $2j$ points [1].

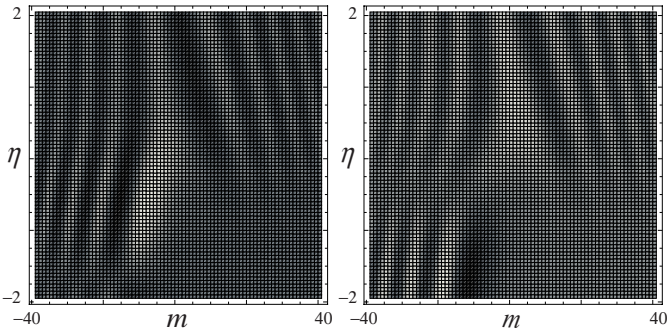

Figure 3. Density plots of the real (*left*) and imaginary (*right*) values of the (finite) discrete repulsive oscillator sub-basis $\Psi^{25}_{\lambda_i,+}(m)$ for 25 positions $m \in \{-12, -11, \ldots, 12\}$, and 25 energies $\{\eta_i\}$ equally spaced between -2 and 2. We see the waves transmitted and reflected by the potential barrier $\sim -\frac{1}{2}m^2$.

In this case, the relations involve the finite oscillator energy number n, now $-\frac{1}{2}+\mathrm{i}(\kappa+\lambda)$, the integer position x now σm and the representation index j now $-k$, $k-1$, corresponding to the finite-dimensional non-unitary representations of so(2,1). The full account of these analytic extensions [27] is quite arduous, so we deem it sufficient to only point them out.

5. Computational issues

The functions in figure 2 should be compared with their continuous counterparts in figure 1. We shall explain now why the vertical axes bear no scale and the horizontal axes have different ranges, and also examine their asymptotic behavior, which lies of course outside the range of the figure.

First, regarding asymptotics we noted under (3) that the continuous repulsive oscillator wavefunctions become at large distances $|x| \to \infty$ a critically decreasing quadratic chirp $\propto \exp(\mathrm{i}\frac{1}{2}x^2)/\sqrt{|x|}$ independent of energy, which is indicative of their Dirac normalization. Correspondingly, in the functions (37) of the discrete model, for far-away points $|m| \gg \kappa, \lambda$, the hypergeometric factor becomes unity while the ratio of Γ's from Stirling's formula behaves as $\propto 1/\sqrt{|m|}$. Chirps are not possible on $\mathcal{Z}$, but examining the limit $|m| \to \infty$ of the recurrence relation (35) we see that the λ-term tends to zero, so that $\Psi^{\kappa}_{\lambda,\pm}(m+1) \approx -\Psi^{\kappa}_{\lambda,\pm}(m-1)$. Thus, instead of a chirp, one has asymptotically a sign alternation between the points m and $m \pm 2$, and thus a wavelength of 4 units.

Regarding the scale for normalization in figure 2, we considered that if these discrete functions are to be used for numerical analysis and synthesis of finite N-point signals, the norm should be computed over the actual range of positions that is being considered, instead of the Dirac norm over $\ell^2(\mathsf{R})$. Correspondingly, instead of a continuum of energies, we should decide on N convenient values $\{\eta_i\}$ chosen to provide and label a basis of N linearly independent N-vectors. We represent this basis (for $N = 81$) in figure 3 through a density plot of the normalized vectors (as we did in [28] for the finite harmonic oscillator). Contained in figure 3 is the assertion that in the expression (37) there is no phase depending on $\kappa - \lambda$. Yet, we cannot expect this basis (and that of left-moving waves) to be orthogonal; to evince its departure from orthogonality, in figure 4 we show the density plot of the $N \times N$ matrix of overlaps $|(\Psi^{\kappa}_{\lambda,+}, \Psi^{\kappa}_{\mu,+})|$, normalized as described above.

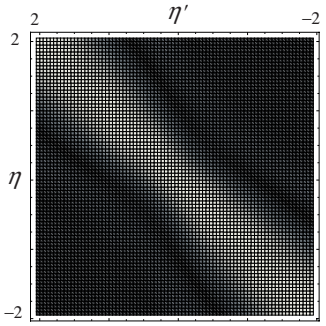

Figure 4. Non-orthogonality of the finite ($N = 25$) discrete repulsive oscillator wavefunctions, seen through their overlaps $\left|\left(\Psi^{25}_{\lambda_i,+}, \Psi^{25}_{\lambda_j,+}\right)\right|$ between the 25 basis vectors, for the 25 equally spaced energies $\eta_i, \eta_j \in [-2, 2]$ of the previous figure.

The horizontal scales in figure 2 have been chosen to show the increasingly good match of $\Psi^{\kappa}_{\lambda,+}(m/\sqrt{\kappa})$, as κ grows, to $\psi_{\lambda,+}(x)$ in figure 1, where the range is $x \in [-8, 8]$, under the contraction (23). The range of points m in the last two columns of the figure has been thus chosen to be $[-8\sqrt{\kappa}, 8\sqrt{\kappa}]$. (The first column of the figure corresponds to a small value of κ, where no contraction is intended, and where the range of m's is adjusted so that the number of maxima be the same as that of the other two columns of discrete functions, and of the continuous functions.) We note that although the absolute values of the discrete wavefunctions (37) in figure 2 clearly tend to the continuous ones (3) in figure 1, the phases that are due to the c^{κ}_{λ}'s in (37) do not; the question of the proper choice of phases for the limit to (3) is mathematically relevant but will not be pursued here. In any case, the multiplication of these discrete wavefunctions by phases $\exp(-\mathrm{i}\eta t)$ will reproduce the features of transmission and reflection that we noted for the continuous repulsive oscillator below (3).

Finally, we should point out that the difference equation (35) relates the values of the solution not only between integer coordinates m, but on any unit-spaced set of points along the continuous coordinate $m \in \mathsf{R}$. The 'discrete' wavefunctions (37) are actually smooth functions of real m when we reinterpret $\mathrm{i}^{\sigma m} \mapsto \exp(\mathrm{i}\sigma \frac{1}{2}\pi m)$ and in (38) and $(-1)^m \mapsto \exp(-\mathrm{i}\sigma\pi m)$.

6. Conclusions

Why should we expect that the discrete repulsive oscillator wavefunctions will resemble the continuous ones? The same question was asked for the discrete harmonic oscillator in [1]. The answer lies in that both systems obey the same geometric and dynamic Hamilton equations, and that the discrete system contracts to the continuous one. However, there are important differences between the harmonic and repulsive oscillators. In the harmonic case, the su(2) representation $j \in \mathcal{Z}^+$ determines the dimension $N = 2j + 1$ of the discrete system and shifts the ground energy through $\eta_n = j + \lambda_n + \frac{1}{2}$, for integer $\lambda_n \in [-j, j]$ being the discrete pseudo-energy. By contrast, in the repulsive case, the contraction (23) does not assign any geometric or dynamical meaning to the representation label $\kappa \in \mathsf{R}$ other than providing the origin of energy through $\eta = \kappa + \lambda$. It seems that the only role of κ is to be a contraction parameter for a family of discrete models. In any case, the conclusion supported by the figures is that the functions (37) do provide a good discrete approximation—better the larger κ is—to the left- and right-moving repulsive oscillator quantum wavefunctions outside the chirp regions, which have additionally a well-behaved analytic extension.

Evidently, the finite position ranges of the computed discrete functions (37) cannot support a Dirac basis for $\ell^2(\mathcal{Z})$ labeled by the continuous energy or pseudo-energy index; figure 4 confirms this statement showing that the overlaps have a rather broad peak along the diagonal, which translates into very small angles between the N-vectors close in energy. The matrix of the basis $\{\Psi^{\kappa}_{\lambda}(m)\}$ for N points m and N energies $\eta = \kappa + \lambda$ in the ranges explored in this paper has a vanishingly small determinant, and the dual basis (amid numerical noise) hardly bears any resemblance to transpose conjugate of the original, as is the case in the mathematical $\ell^2(\mathcal{Z})$ formalism. In the finite harmonic oscillator, where approximate bases (such as that of sampled Hermite–Gauss functions [29–31]) can be subject to a Schmidt orthogonalization process from the ground state up, a discrete repulsive oscillator basis may be orthogonalized over selected discrete energies $\eta_n \geqslant 0$ for right-moving free states to form a Gaussian-like packet, or $\eta_n \leqslant 0$ for states that collide, reflect and transmit through the potential barrier. Whether this process is satisfactory or not depends on the application of the model.

Finally, following the lead of su(2) systems, whose phase space is a sphere [32, 33], we expect that the phase space of infinite discrete systems will be a one-sheeted hyperboloid; and there, an so(2,1)-covariant Wigner function can be set up. These and other questions will be developed in a forthcoming paper.

Acknowledgments

We acknowledge the support of the *Óptica Matemática* projects (DGAPA-UNAM IN-105008 and SEP-CONACYT 79899), and we thank Guillermo Krötzsch (ICF-UNAM) for his indispensable help with the graphics.

References

[1] Atakishiyev N M and Wolf K B 1997 Fractional Fourier-Kravchuk transform *J. Opt. Soc. Am.* A **14** 1467–77
[2] Atakishiyev N M, Pogosyan G S and Wolf K B 2005 Finite models of the oscillator *Phys. Part. Nuclei* (Suppl 3) **36** 521–55
[3] Vicent L E and Wolf K B 2008 Unitary transformation between Cartesian- and polar-pixellated screens *J. Opt. Soc. Am.* A **25** 1875–84
[4] Wolf K B 2008 Linear transformations and aberrations in continuous and in finite systems *J. Phys. A: Math. Theor.* **41** 304026 (19 pp)
[5] Nieto L M, Atakishiyev N M, Chumakov S M and Wolf K B 1998 Wigner distribution function for Euclidean systems *J. Phys. A: Math. Gen.* **31** 3875–95
[6] Bargmann V 1947 Irreducible unitary representations of the Lorentz group *Ann. Math.* **48** 568–642
[7] Naĭmark M A 1964 *Linear Representations of the Lorentz Group* (Oxford: Pergamon)
[8] Gel'fand I M, Graev M I and Vilenkin N Ya 1966 *Generalized Functions* vol 5 (New York: Academic)
[9] Barton G 1986 Quantum mechanics of the inverted oscillator potential *Ann. Phys. (NY)* **166** 322–63
[10] Balazs N L and Voros A 1990 Wigner's function and tunneling *Ann. Phys. (NY)* **199** 123–40
[11] Wolf K B 1979 *Integral Transforms in Science and Engineering* (New York: Plenum)
[12] Kalnins E G and Miller W Jr 1974 Lie theory and separation of variables: 5. The equations $\mathrm{i}U_t + U_{xx} = 0$ and $\mathrm{i}U_t + U_{xx} - c/x^2U = 0$ *J. Math. Phys.* **15** 1728–35
[13] Baskoutas S, Jannussis A, Mignani R and Papatheou V 1993 Tunnelling process for non-Hermitian systems: the complex-frequency inverted oscillator *J. Phys. A: Math. Gen.* **26** L819–24
[14] Heller E J 1999 The many faces of tunneling *J. Chem. Phys.* A **103** 10433–44
[15] Pedrosa I A and Guedes I 2004 Quantum states of a generalized time-dependent inverted harmonic oscillator *Int. J. Mod. Phys.* B **18** 1379–85
[16] Müller-Kirsten H J W 2006 *Introduction to Quantum Mechanics* (Singapore: World Scientific)
[17] Yuce C, Kiliç A and Coruh A 2006 Inverted oscillator *Phys. Scr.* **74** 114–6
[18] Erdélyi A, Magnus W, Oberhettinger F and Tricomi F G 1953 *Higher Transcendental Functions* vol 2 (New York: McGraw-Hill)

[19] Abramowitz M and Stegun I A (eds) 1964 *Handbook of Mathematical Functions* (Washington DC: National Bureau of Standards)
[20] Sánchez Mondragón J and Wolf K B (eds) 1986 *Lie Methods in Optics (Lecture Notes in Physics* vol 250) (Heidelberg: Springer) appendix B
[21] Lindblad G and Nagel B 1970 Continuous bases for unitary irreducible representations of $SU(1, 1)$ *Ann Inst. Henri. Poincaré* A **13** 27–56
[22] Biedenharn L C and Louck J D 1981 *Angular Momentum in Quantum Physics. Encyclopedia of Mathematics and Its Applications* ed G-C Rota (Reading, MA: Addison-Wesley)
[23] Atakishiyev N M, Nagiyev Sh M, Vicent L E and Wolf K B 2000 Covariant discretization of axis-symmetric linear optical systems *J. Opt. Soc. Am.* A **17** 2301–14
[24] Basu D and Wolf K B 1982 The unitary irreducible representations of SL(2,*R*) in all subgroup reductions *J. Math. Phys.* **32** 189–205
[25] Mukunda N and Radhakrishnan B 1974 Clebsch–Gordan problem and coefficients for the three-dimensional Lorentz group in a continuous basis *J. Math. Phys.* **15** 1320–35
[26] Gradshteyn I S and Ryzhik I M 2000 *Table of Integrals, Series, and Products* 6th edn (New York: Academic)
[27] Drechsler W 1986 Complex angular momentum theory in particle physics *Fortschr. Phys.* **18** 305–448
[28] Wolf K B and Krötzsch G 2007 Geometry and dynamics in the fractional discrete Fourier transform *J. Opt. Soc. Am.* A **24** 651–8
[29] Pei S-C and Yeh M-H 1997 Improved discrete fractional transform *Opt. Lett.* **22** 1047–9
[30] Wolf K B 2009 Mode analysis and signal restoration with Kravchuk functions *J. Opt. Soc. Am.* A **26** 509–16
[31] Namias V 1980 The fractional order Fourier transform and its application to quantum mechanics *J. Inst. Math. Appl.* **25** 241–65
[32] Atakishiyev N M, Chumakov S M and Wolf K B 1998 Wigner distribution function for finite systems *J. Math. Phys.* **39** 6247–61
[33] Ali S T, Atakishiyev N M, Chumakov S M and Wolf K B 2000 The Wigner function for general Lie groups and the wavelet transform *Ann. Henri Poincaré* **1** 685–714